Article

Journal of
Nanoscience and Nanotechnology
Vol. 19, 1301–1307, 2019
www.aspbs.com/jnn

Effects of the Process Parameters on the Properties of Sputter-Deposited Tin Oxide Thin Films

Sang Woo Woo[1], Han Byeol Seo[1], Jinsung Choi[1], Byung Seong Bae[2], and Eui-Jung Yun[3,*]

[1] Department of NanoBio Tronics, Hoseo University, Asan, Chungnam 31499, Republic of Korea
[2] Department of Display Engineering, Hoseo University, Asan, Chungnam 31499, Republic of Korea
[3] Department of ICT Automotive Engineering, Hoseo University, Dangjin, Chungnam 31702, Republic of Korea

This study examined the effects of the oxygen partial pressure on the properties of tin oxide (SnO_x) thin films deposited by radio frequency magnetron sputtering using a SnO target. The properties of the samples were characterized by Hall Effect measurements, dynamic-secondary ion mass spectrometry, X-ray photoelectron spectroscopy (XPS), X-ray diffraction, and atomic force microscopy. All the samples exhibited dominant Sn^{2+} XPS peaks, indicating that SnO with *p*-type conductivity was the main composition regardless of the oxygen partial pressure. The samples deposited with an oxygen partial pressure of 12% showed the best *p*-type characteristics, which included a maximum hole mobility of 1.94 cm^2/Vs, carrier concentration of $3.83 \times 10^{17}/cm^3$, Sn^{2+} peak area percentage of 91.34%, Sn^{4+} peak area percentage of 2.35%, and Sn^0 peak area percentage of 6.31%. As the oxygen partial pressure was increased to more than 12%, the Sn^{2+} peak area percentage decreased while the Sn^{4+} peak area percentage increased. This was attributed to the reduction of the SnO phase and the growth of the SnO_2 phase in the samples due to the incorporation of more oxygen. These results are expected to contribute to the development of *p*-type SnO-based TFTs with good performance.

Keywords: Tin Oxide (SnO) Thin-Films, Sputtering, Process Parameters, Sn^{2+} Peak Area Percentage.

1. INTRODUCTION

Recently, oxide thin-film transistors (TFTs) have been limited to *n*-channel devices because oxide semiconductors (OSs) are mainly *n*-type. *n*-Type OSs have large electron mobility because their electron transporting paths [conduction band minima (CBM)] are formed mainly from the isotropic and delocalized *s* orbitals of metal cations, whereas *p*-type OSs have low hole mobility because their hole conduction paths (valence band maxima (VBM)) consist mainly of anisotropic and strongly localized 2*p* orbitals of oxygen ions.[1–13] On the other hand, transparent complementary metal oxide semiconductor (CMOS) circuits, which is a key element to fuel the microelectronics revolution by offering great advantages over *n*-channel MOS (NMOS), such as low power dissipation and higher density of logic functions on a chip, can be realized if both high performance *n*- and *p*-type oxide TFTs can be developed.[4, 11, 12, 14–20] As a result, an exploration of high performance *p*-type OSs is an essential issue for the development of giant microelectronics.

Tin monoxide (SnO) is one of the most attractive *p*-type OS with high hole mobility owing to its Sn 5s nature at the VBM.[1, 2, 4, 6–13] The spatially spread and spherical Sn 5s orbitals, which are hybridized with O 2*p* orbitals to form pseudo-closed ns^2 orbitals at the VBM, are isotropic, resulting in high hole mobility by reducing the localization of the VBM. SnO thin films have been prepared using various techniques, such as pulsed laser deposition,[1, 3] evaporation,[2, 12] radio frequency (RF) or direct current (DC) sputtering,[5–11, 13, 15–17, 19–22] solution processes,[23] and physical vapor deposition.[18] Among them, sputtering is the most effective process to fabricate large area devices and can produce multi-state oxides, such as *p*-type SnO, *n*-type SnO_2, and metallic Sn.[13] Understanding these multi-states is essential because a phase impurity always impedes the control of the film performance. In addition, an increase in the number of oxygen atoms within the SnO thin films results in an increase in Sn^{4+}

*Author to whom correspondence should be addressed.

Table I. Summary of the Hall Effect measurement results for the series of samples prepared in this study.

Oxygen ratio of samples (%)	Resistivity ($\Omega \cdot$cm)	Hall mobility [$cm^2/(V \cdot s)$]	Carrier concentration ($1/cm^3$)
0	Immeasurable owing to very high resistance		
8	28.69	0.289	7.51×10^{17}
12	9.154	1.94	3.51×10^{17}
16	40.12	0.109	1.43×10^{18}
20	39.25	0.0185	8.58×10^{18}

ions, giving the film *n*-type conductivity, which in turn degrades the device performance.[24] Nevertheless, details of the properties of sputter-deposited SnO_x thin films are unclear and the device properties of SnO-based TFTs are still far from acceptable for practical applications. Furthermore, there are few reports on the effects of the sputtering process parameters on the properties of SnO_x thin films deposited using a SnO sputtering target. Therefore, this study examined the effects of important parameters, such as the oxygen partial pressure and film thickness on the properties of sputter-deposited SnO_x thin films using a SnO sputtering target.

2. EXPERIMENTAL DETAILS

SnO_x thin films were deposited on 400-μm-thick Si or glass substrates at room temperature (RT) using a SnO (99.999%, 2 inch diameter) sputtering target under the following conditions: a radio frequency (RF) power of 50 W, working pressure of 0.533 Pa, and oxygen ratios of 0 to 20%. Pure argon (99.999%) and oxygen gas mixtures were used as the reaction gas and the total flow rate was 25 sccm. The target-to-substrate distance was kept constant at 10 cm for all depositions. The substrate was rotated at 13 rpm to deposit the SnO_x thin films with a uniform thickness. The SnO_x film thickness was increased from 58 to 181 nm by decreasing the oxygen ratio.

The contents (at.%) and chemical bonding states of Sn and O in the SnO_x thin films were analysed by X-ray photoelectron spectroscopy (XPS). The changes in the depth profiles of Sn, Si, and O in the samples were examined by dynamic secondary ion mass spectrometry (D-SIMS). The electrical properties of SnO_x thin films were measured at RT using a Hall Effect measurement system according to a van der Pauw configuration after forming the Ohmic contacts with a 100-nm-thick Al layer using a sputtering system, followed by alloying at 150 °C in air for 1 hour. The structures and surface morphologies of the films were characterized by X-ray diffraction (XRD) with a Cu Kα_1 radiation source ($\lambda = 0.15406$ nm) and atomic force microscopy (AFM, nanoscope IV multimode), respectively.

3. RESULTS AND DISCUSSION

Table I lists the Hall Effect measurements, which revealed the electrical properties of a series of samples prepared in this study. All samples exhibited *p*-type conductivity, regardless of the oxygen ratio. At oxygen ratios of 0–12%, the product of the mobility (μ) and hole carrier concentration (p) increased with increasing oxygen ratio, resulting in a decrease in resistivity (ρ), as listed in Table I. In contrast, those of the product decreased with increasing oxygen ratio, resulting in an increase in ρ for oxygen ratios in the range of 12–20%. This result followed the equation,

$$\rho = \frac{1}{pq\mu} \tag{1}$$

where q is the charge of an electron. In the case of oxygen ratios in range of 0–12%, the large increase in μ with increasing oxygen ratio was attributed mainly to a decrease in ρ owing to a decrease in the amount of carrier scattering by the reduced defect and carrier concentrations. On the other hand, an opposite argument was applicable for oxygen ratios in range of 12–20%. A large increase in the oxygen ratio causes an increase in the defect and carrier densities in thinner SnO_x, resulting in a large increase in carrier scattering, which increases ρ and in turn decreases μ. Note that the diffusion of oxygen into the SnO_x films produced in-band gap defects and caused an increase in resistance.[24] This suggests that the high resistance of SnO_x thin films prepared at oxygen concentrations of 12–20% is related to the introduction of O into the SnO_x thin films. As indicated in Table I, the SnO_x thin films deposited with an oxygen ratio of 12% showed the best electrical properties, which includes a Hall mobility of 1.94 $cm^2/(V \cdot s)$, a hole carrier concentration of 3.51×10^{17} $1/cm^3$, and a resistivity of 9.154 $\Omega \cdot$cm.

The SIMS depth profiles (Fig. 1) exhibit typical intensity variations in Sn, O, and Si concentrations in the SnO_x thin films prepared at different oxygen ratios. As shown in Figure 1, the SnO_x film thickness decreased from 181 to 58 nm with increasing oxygen ratio from 0 to 20%. During the deposition process, sputtered Sn and O atoms ejected from the target by energetic sputtering Ar atoms can deposit on the substrates. At higher oxygen ratios, the collision of the sputtered atoms with the oxygen atoms increases, resulting in the deposition of thinner oxide films on the substrates. In the case of the samples deposited at oxygen concentrations of 0–12%, the composition of the samples was close to the *p*-type tin monoxide (SnO). This supports the Hall Effect measurements in that the samples deposited with oxygen ratios in range of 0–12% exhibited *p*-type conductivity. When the samples are deposited with low oxygen ratios in range of 0–12% by a mono-SnO ceramic target instead of a Sn metallic target, the chemical reaction between sputtered Sn and O atoms before coating the substrate is minimized. The deposited film is therefore similar to the target material, which cause the SnO composition in samples deposited with oxygen ratios in range of 0–12%.

On the other hand, as shown in Figure 1, in the case of the samples deposited with oxygen concentrations of

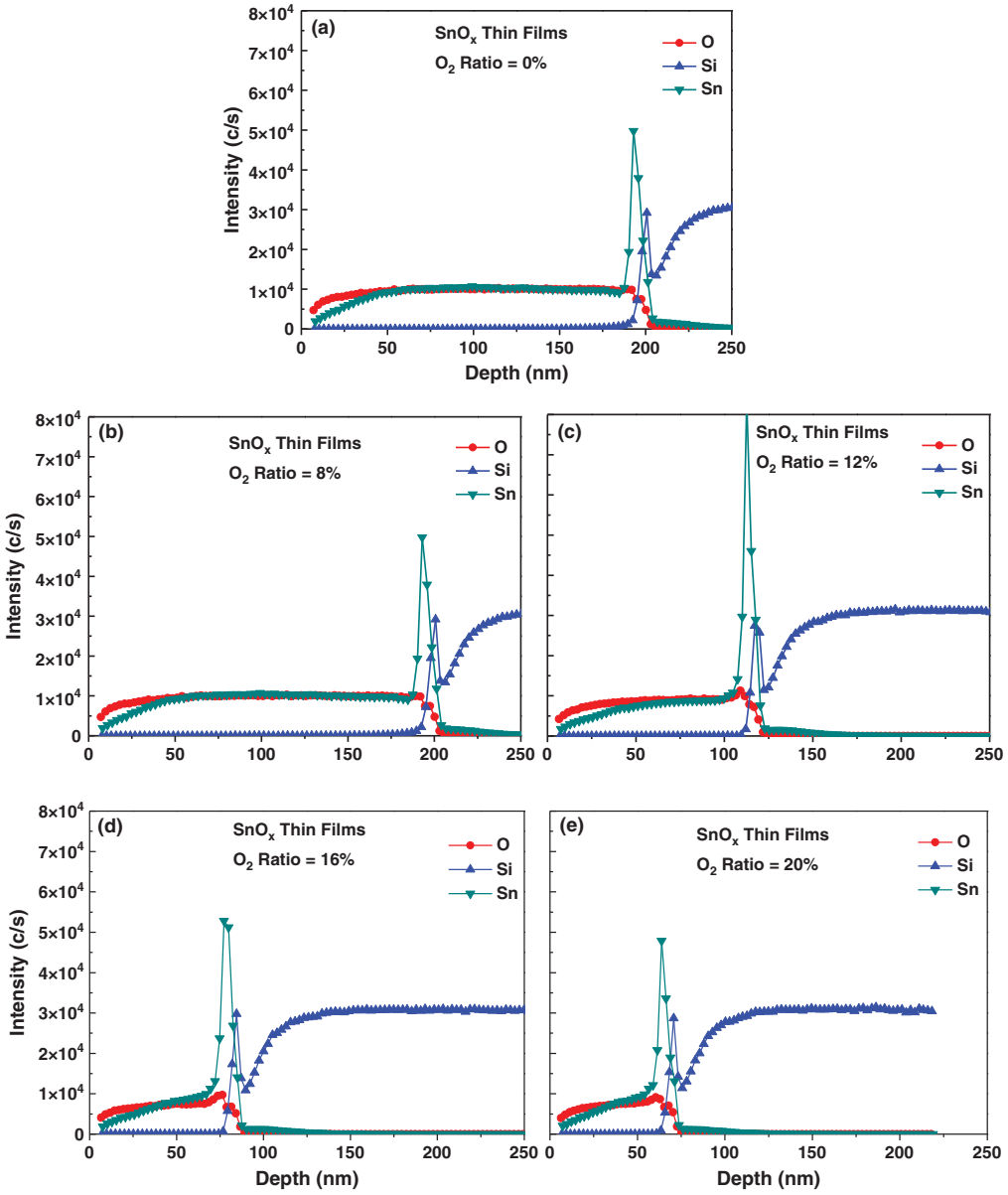

Figure 1. Intensity variations in the tin (Sn), oxygen (O), and silicon (Si) concentrations in the SnO_x thin films prepared at oxygen ratios of (a) 0, (b) 8, (c) 12, (d) 16, and (e) 20%, which were obtained from the SIMS depth profiles.

12–20%, a larger amount of O diffused into the SnO_x thin films with a thinner thickness during deposition with increasing oxygen concentration. Therefore, the increased O concentration apparently causes unbalanced concentrations in Sn and O and an increase in the number of O-related defects. Consequently, the O concentration is higher than that of Sn in the SnO_x surface while it is lower than that of Sn near the SnO/Si interface, which in turn results in a multi-states oxide, such as *p*-type SnO, *n*-type SnO_2, and metallic Sn, in the case of the samples deposited at oxygen concentrations of 12–20%, as shown in Figure 1.

Figure 2 shows the XRD patterns of SnO_x films deposited at various oxygen ratios. At room substrate temperature, the adatom mobility and the reaction between Sn and O are restricted on the substrate surface, which results in a large number of defects in SnO_x films. Therefore, very fine nanocrystalline or amorphous films are formed. As shown in Figure 2, the samples with an oxygen ratio of 0% revealed a single halo peak centered at ~29° 2θ, while

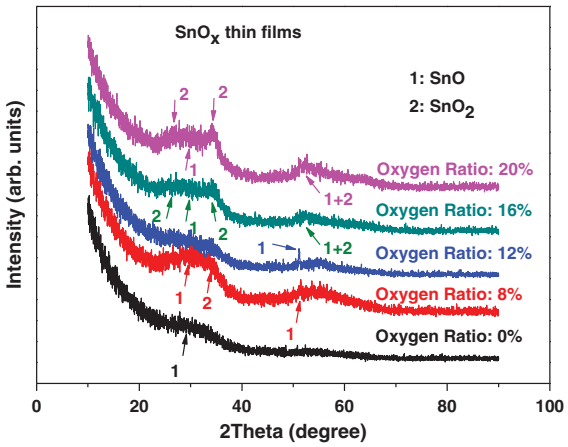

Figure 2. X-ray diffraction (XRD) patterns of SnO_x films that were deposited at various oxygen ratios.

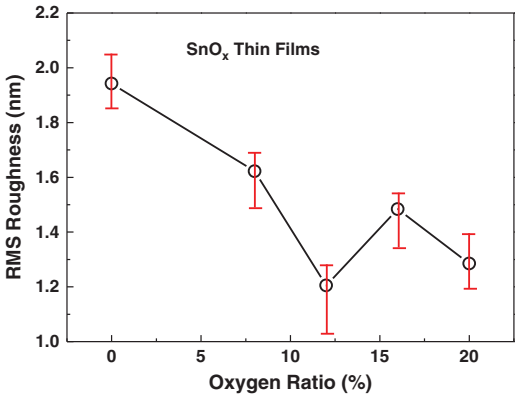

Figure 4. Root mean square (RMS) of surface roughness of SnO_x films prepared by various oxygen ratios.

those with oxygen ratios of 8 and 12% showed two halo peaks centered at ~29° and ~51° 2θ, respectively. These two halos can have two SnO and SnO_2 phases because they are very broad. However, the peak positions of these halos are apparently identical to those observed from a tetragonal SnO phase.[11, 13, 18–20] This suggests that the samples with oxygen ratios of 0–12% are mainly the *p*-type SnO phase, as confirmed by the Hall and SIMS results. On the other hand, as the oxygen ratio was increased further to 16 and 20%, three additional broad XRD peaks at ~26.3, ~34.3, and ~52.5° 2θ, corresponding to the (110), (101), and (211) orientations of nanocrystalline SnO_2, respectively, were obtained.[8, 9, 11, 21, 22] This suggests that in the case of the samples deposited with oxygen ratios higher than 12%, the *n*-type SnO_2 phase grows and multi-phases, such as SnO, SnO_2, and Sn, coexist in the SnO_x films, as shown in Figures 1 and 2.

Figures 3 and 4 show AFM images and the root mean square (RMS) of the surface roughness of SnO_x films as a function of the oxygen ratio, respectively. In Figure 4, we inserted the statistical bars to verify our reproducible data. The surface roughness of the SnO_x films changed

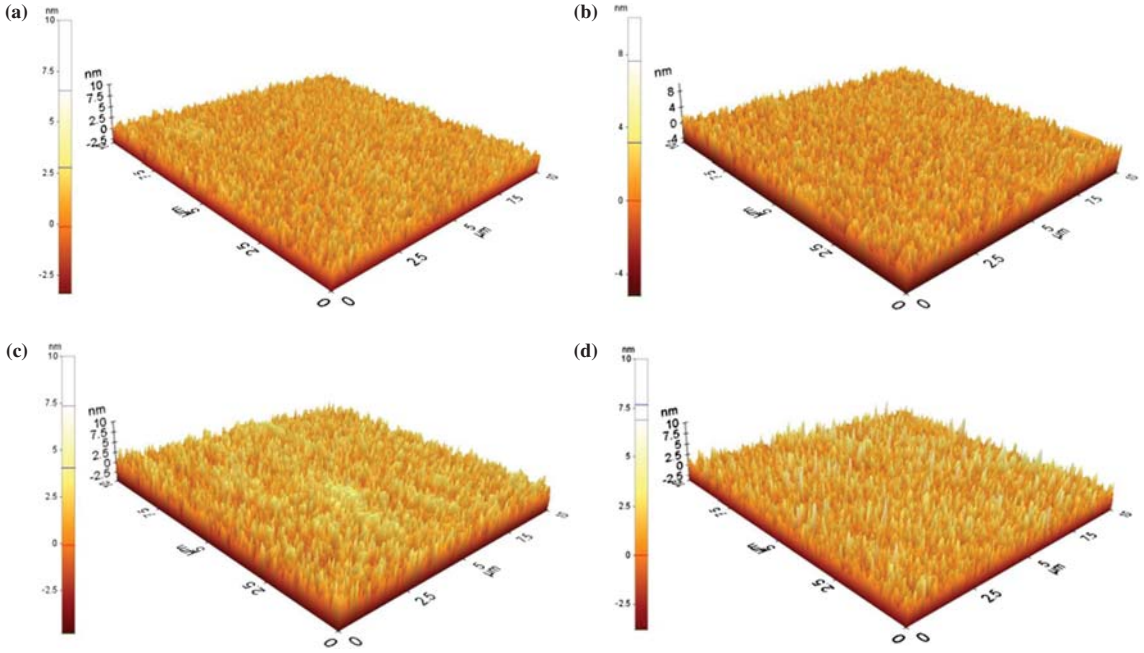

Figure 3. AFM images of SnO_x films prepared at various oxygen ratios as a function of oxygen ratio; (a) oxygen ratio = 8% (RMS roughness = 1.622 nm), (b) oxygen ratio = 12% (RMS roughness = 1.205 nm), (c) oxygen ratio = 16% (RMS roughness = 1.484 nm), and (d) oxygen ratio = 20% (RMS roughness = 1.285 nm).

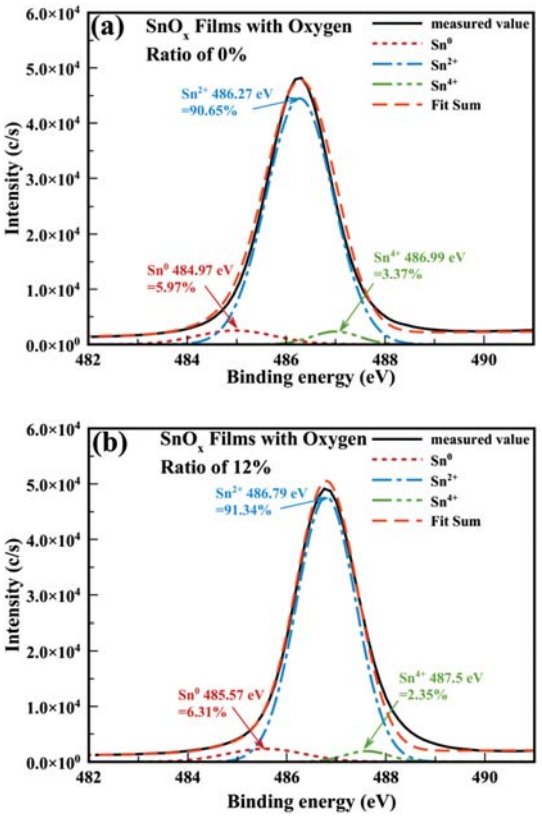

Figure 5. Typical Sn $3d_{5/2}$ narrow-scan XP spectra fitted using three Gaussian peaks for the SnO_x thin films prepared at oxygen ratios of (a) 0 and (b) 12%.

notably with increasing oxygen ratio. As shown in Figure 4, the RMS decreased continuously with increasing oxygen ratio, reaching the minimum value at an oxygen concentration of 12%, and increased suddenly with further increases in the oxygen concentration. The decrease in surface roughness also resulted in an increase in the conducting path in the films and a decrease in the effective surface area of films as well as the number of absorption sites for oxygen, which lead to a decrease in film resistivity.[25] Therefore, the smoothest surface morphology observed in the films prepared at an oxygen concentration of 12% will result in the lowest resistivity in those films, as shown in Table I.

All binding energies determined by XPS were calibrated using the carbon (C) 1*s* reference peak at 284.6 eV. Two Sn 3*d* narrow-scan XPS peaks for the SnO_x thin films were observed at binding energies of 486.3 and 494.7 eV, which are related to the spin orbit of Sn $3d_{5/2}$ and Sn $3d_{3/2}$, respectively.[8, 9, 11, 13, 18, 19, 21, 23] The Sn $3d_{5/2}$ narrow-scan XP spectra of the SnO_x thin films were fitted using three Gaussian peaks (GPs) associated with the Sn^0, Sn^{2+}, and Sn^{4+} peaks centered at approximately 485–485.6, 486.2–486.8, and 486.9–487.6 eV, which represent metallic Sn, *p*-type SnO, and *n*-type SnO_2, respectively.

Figures 5(a) and (b) present typical examples of the Sn $3d_{5/2}$ narrow-scan XP spectra fitted using three GPs in the samples prepared at oxygen ratios of 0 and 12%, respectively. The fitting of the Sn $3d_{5/2}$ peaks using three GPs was outstanding. As shown in Figure 5(a), for the SnO_x films prepared at an oxygen ratio of 0%, the percentage areas of the Sn^0 peaks centered at approximately 485 eV, Sn^{2+} peaks at 486.3 eV, and Sn^{4+} peaks at 487 eV were 5.97, 90.65, and 3.37%, respectively. Figure 5(b) also shows that the percentage areas of the Sn^0 peaks centered at approximately 485.6 eV, Sn^{2+} peaks at 486.8 eV, and Sn^{4+} peaks at 487.5 eV were 6.31, 91.34, and 2.35%, respectively, for the SnO_x thin films prepared at an oxygen concentration of 12%.

Figure 6 shows the percentage areas of the three GPs as a function of the oxygen concentration for the samples prepared at various oxygen gas ratios, which were obtained after fitting the Sn $3d_{5/2}$ peaks using the three Sn^0, Sn^{2+}, and Sn^{4+} GPs, as shown in Figure 5. As shown in Figure 6, for the samples prepared with oxygen ratios of 0–12%, the Sn^{2+} peak area was dominant and almost unchanged with increasing oxygen ratio, which suggests that the in-diffusion of O from the chamber to the sample surface decelerates during deposition, as confirmed by Table I and Figures 1, 2, and 4. As the oxygen ratio was increased to more than 12%, the Sn^{2+} peak area percentage decreased while the Sn^{4+} peak area percentage increased, which were associated with a decrease in the SnO phase and an increase in the SnO_2 phase in the samples, respectively, due to the incorporation of more oxygen. This is in agreement with a recent report showing that an increase in the amount of oxygen within the SnO thin films results in an increase in the Sn^{4+} ions.[24] Figure 6 also shows that the *p*-type SnO was the main composition regardless of the change in oxygen ratio. The samples

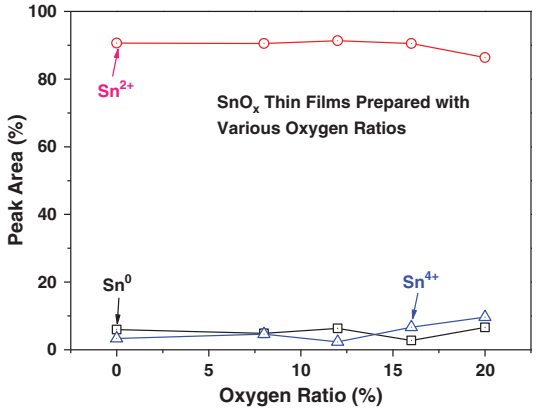

Figure 6. Percentage area characteristics of three Gaussian peaks as a function of the oxygen ratio obtained from the Sn $3d_{5/2}$ narrow scan XP spectra of SnO_x thin films prepared with various oxygen ratios. This result was obtained after fitting the $3d_{5/2}$ peaks using the three Sn^0, Sn^{2+}, and Sn^{4+} Gaussian peaks, as shown in Figure 5.

deposited with an oxygen ratio of 12% showed the best *p*-type characteristics, which included the Sn^{2+} peak area percentage of 91.34%, the Sn^{4+} peak area percentage of 2.35%, and the Sn^{0} peak area percentage of 6.31%.

The O 1*s* narrow-scan XP spectra of the SnO_x thin films were also fitted using three GPs related to the low, middle, and high peaks (LP, MP, and HP) centered at approximately 529.8–530.1, 531–531.1, and 531.6–531.9 eV, respectively. The LP was assigned to O^{2-} ions surrounded by Sn and O metal atoms in a fully oxidized stoichiometric SnO_x system. The MP can also be associated with O^{2-} ions in the oxygen-deficient regions within the SnO_x matrix and is related to V_o defects, whereas HP is related to chemisorbed or dissociated oxygen or to O–H bonding near the film surface.[26–29]

Figures 7(a) and (b) present typical examples of the O 1*s* narrow-scan XP spectra fitted using the LP, MP, and HP GPs in the samples prepared at oxygen ratios of 0 and 12%, respectively. The fitting of the O 1*s* peaks using the three LP, MP, and HP GPs was excellent. As shown in Figure 7(a), for SnO_x films prepared at oxygen ratios of 0%, the percentage areas of LP centered at approximately 530 eV, MP at 530.96 eV, and HP at 531.94 eV were

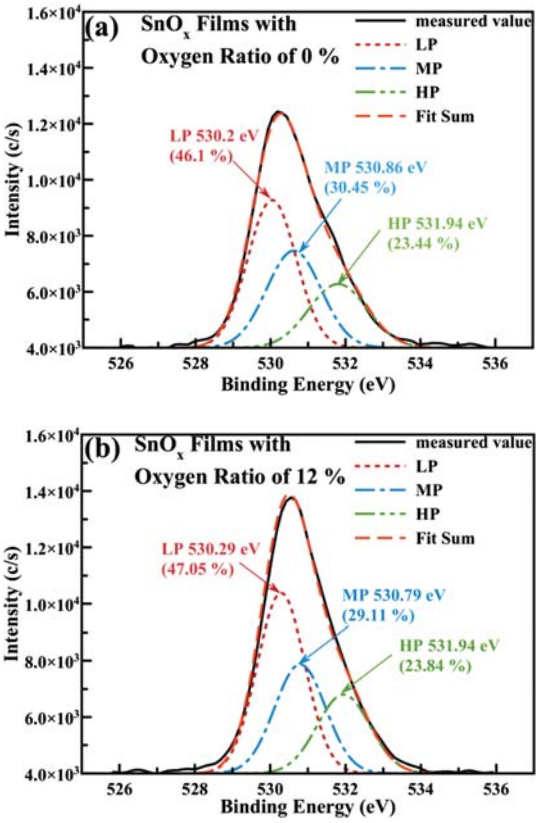

Figure 7. Typical O 1*s* narrow-scan XP spectra fitted using three LP, MP, and HP Gaussian peaks for the SnO_x thin films prepared with oxygen ratios of (a) 0 and (b) 12%.

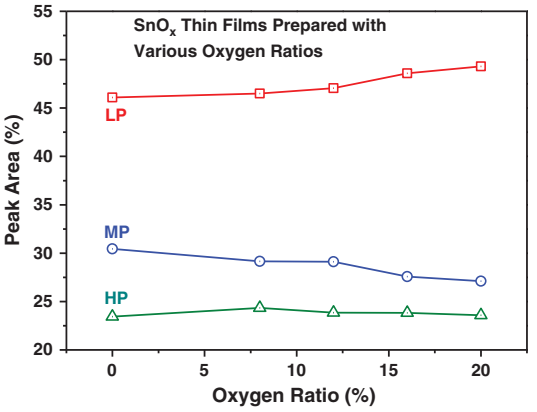

Figure 8. Percentage area characteristics of three Gaussian peaks as a function of the oxygen ratio obtained from the O1*s* narrow scan XP spectra of SnO_x thin films prepared at various oxygen ratios. This result was obtained after fitting the O 1*s* peaks using the three LP, MP, and HP Gaussian peaks, as shown in Figure 7.

45.57, 30.45, and 23.98%, respectively. On the other hand, Figure 7(b) shows that the percentage areas of LP centered at approximately 530.63 eV, MP at 530.91 eV, and HP at 532.01 eV were 48.15, 29.11, and 22.74%, respectively, for the SnO_x thin films prepared at an oxygen ratio of 12%.

Figure 8 also shows the percentage areas of the three GPs as a function of the oxygen ratio for the samples prepared at various oxygen ratios, which were obtained after fitting the O 1*s* peaks using the three LP, MP, and HP GPs, as shown in Figure 7. In the case of the samples with oxygen ratios of 0–12 %, with increasing oxygen ratio, the LP and MP areas increased and decreased slightly, respectively, which indicates that the in-diffusion of O to the sample surface is retarded during sample deposition, as listed in Table I and Figures 1, 2, 4, and 6. On the other hand, for the samples with oxygen ratios greater than 12%, the LP and MP increased and decreased notably with increasing oxygen ratio areas, respectively. The decrease in MP area can be explained by the following argument. When the SnO_x thin films were prepared at oxygen ratios greater than 12%, the in-diffusion of O from the chamber into the film increased with increasing oxygen ratio, resulting in the annihilation of oxygen vacancies (V_o) in the films, which causes a decrease in the number of V_o. The increase in LP area for the samples with oxygen ratios greater than 12% was also related to the enhancement of the reaction of Sn metal with O due to in-diffused O, as confirmed by Table I and Figures 1, 2, 4, and 6. As indicated in Figure 8, however, the HP area was almost constant at approximately 23.8%, regardless of the change in oxygen ratio. This suggests that the same amount of O or H appears near the surfaces of the SnO_x thin films.

4. CONCLUSION

This study examined the effects of parameters, such as the oxygen partial pressure and film thickness on the

properties of sputter-deposited SnO_x thin films using a SnO sputtering target. For the samples with oxygen ratios of 0–12%, the in-diffusion of O from the chamber to the sample surface was retarded during deposition, as confirmed by the Hall Effect, SIMS, XRD, and XPS results. This reduced the defect and carrier concentrations in the SnO_x thin films, resulting in a decrease in carrier scattering and a decrease in resistivity, which in turn increased the mobility of the samples significantly. On the other hand, in the case of samples with oxygen ratios higher than 12%, the in-diffusion of O from the chamber to the sample surface accelerates during film deposition, which enhanced the defect and carrier concentrations in the thinner SnO_x thin films. This caused an increase in carrier scattering and an increase in resistivity, giving rise to a decrease in the mobility of the samples. The Hall Effect, SIMS, XRD, and XPS results showed that all samples showed the *p*-type conductivity regardless of oxygen ratio. The samples deposited with an oxygen ratio of 12% showed the best *p*-type characteristics, which include a maximum hole mobility of 1.94 cm^2/Vs; carrier concentration of $3.83 \times 10^{17}/cm^3$; and Sn^{2+}, Sn^{4+}, and Sn^0 peak area percentages of 91.34, 2.35, and 6.31%, respectively.

Acknowledgments: This research was supported by the Academic Research Fund of Hoseo University in 2017 (20170049).

References and Notes

1. Y. Ogo, H. Hiramatsu, K. Nomura, H. Yanagi, T. Kamiya, M. Hirano, and H. Hosono, *Appl. Phys. Lett.* 93, 032113 (**2008**).
2. L. Y. Liang, Z. M. Liu, H. T. Cao, Z. Yu, Y. Y. Shi, A. H. Chen, H. Z. Zhang, Y. Q. Fang, and X. L. Sun, *J. Electrochem. Soc.* 157, H598 (**2010**).
3. K. Nomura, T. Kamiya, and H. Hosono, *Adv. Mater.* 23, 3431 (**2011**).
4. E. Fortunato, P. Barquinha, and R. Martins, *Adv. Mater.* 24, 2945 (**2012**).
5. J. Um, B. M. Roh, S. Kim, and S. E. Kim, *Mater. Sci. Semicond. Process.* 16, 1679 (**2013**).
6. P. C. Hsu, W. C. Chen, Y. T. Tsai, Y. C. Kung, C. H. Chang, C. J. Hsu, C. C. Wu, and H. H. Hsieh, *Jpn. J. Appl. Phys.* 52, 05DC07 (**2013**).
7. P. C. Hsu, W. C. Chen, Y. T. Tsai, Y. C. Kung, C. H. Chang, C. C. Wu, and H. H. Hsieh, *Thin Solid Films* 555, 57 (**2014**).
8. S.-S. Lin, Y.-S. Tsai, and K.-R. Bai, *Appl. Surf. Sci.* 380, 203 (**2016**).
9. S.-S. Lin, S.-Y. Fan, and Y.-S. Tsai, *Ceram. Int.* 43, 1802 (**2017**).
10. H.-J. Kim, C.-Y. Jeong, S.-D. Bae, J.-H. Lee, and H.-I. Kwon, *IEEE Electron Dev. Lett.* 38, 473 (**2017**).
11. L. Guo, M. Zhao, D. Zhuang, Q. Gong, H. Tan, M. Cao, and L. Ouyang, *Mater. Sci. Semicond. Process.* 46, 35 (**2016**).
12. L. Qiang, W. Liu, Y. Pei, G. Wang, and R. Yao, *Solid-State Electronics* 129, 163 (**2017**).
13. A. H.-T. Nguyen, M.-C. Nguyen, J. Choi, S. Han, J. Kim, and R. Choi, *Thin Solid Films* 641, 24 (**2017**).
14. R. Martins, A. Nathan, R. Barros, L. Pereira, P. Barquinha, N. Correia, R. Costa, A. Ahnood, I. Ferreira, and E. Fortunato, *Adv. Mater.* 23, 4491 (**2011**).
15. C. Ju, C. Park, H. Yang, U. Kim, Y. M. Kim, and K. Char, *Curr. Appl. Phys.* 16, 300 (**2016**).
16. J.-H. Lee, Y.-J. Choi, C.-Y. Jeong, D.-K. Jung, S. Ham, and H.-I. Kwon, *IEEE Electron Dev. Lett.* 37, 300 (**2016**).
17. A. Azmi, J. Lee, T. J. Gim, R. Choi, and J. K. Jeong, *IEEE Electron Device Letters* 38, 1543, DOI 10.1109/LED.2017.2758349.
18. P.-C. Chen, Y.-C. Chiu, Z.-W. Zheng, C.-H. Cheng, and Y.-H. Wu, *J. Alloys Compd.* 707, 162 (**2017**).
19. H. Luo, L. Liang, and H. Cao, *Solid-State Electronics* 129, 88 (**2017**).
20. J. S. Ahn, R. Pode, and K. B. Lee, *Thin Solid Films* 608, 102 (**2016**).
21. J. Yang, S. Pi, Y. Han, R. Fu, T. Meng, and Q. Zhang, *IEEE Trans. Electron Devices* 63, 1904 (**2016**).
22. B. L. Zhu, X. Zhao, W. C. Hu, T. T. Li, J. Wu, Z. H. Gan, J. Liu, D. W. Zeng, and C. S. Xie, *J. Alloys Compd.* 719, 429 (**2017**).
23. D. M. Priyadarshini, R. Mannam, M. S. R. Rao, and N. DasGupta, *Appl. Surf. Sci.* 418, 414 (**2017**).
24. H. Luo, L. Y. Liang, H. T. Cao, M. Z. Dai, Y. C. Lu, and M. Wang, *ACS Appl. Mater. Interf.* 7, 17023 (**2015**).
25. T. Ratana, P. Amornpitoksuk, T. Ratana, and S. Suwanboon, *J. Alloys Compd.* 470, 408 (**2009**).
26. C.-H. Hung, S.-J. Wang, P.-Y. Liu, C.-H. Wu, H.-P. Yan, N.-S. Wu, and T.-H. Lin, *Mater. Sci. Semicond. Process.* 67, 84 (**2017**).
27. H. Xie, J. Xu, G. Liu, L. Zhang, and C. Dong, *Mater. Sci. Semicond. Process.* 64, 1 (**2017**).
28. M.-H. Kim, M.-J. Choi, K. Kimura, H. Kobayashi, and D.-K. Choi, *Solid-State Electronics* 126, 87 (**2016**).
29. Y.-H. Joo and C.-I. Kim, *Thin Solid Films* 583, 40 (**2015**).

Received: 9 January 2018. Accepted: 19 March 2018.